Nuclear Science and Techniques (2025) 36:13
https://doi.org/10.1007/s41365-024-01567-2

Failure mechanisms of AlGaN/GaN HEMTs irradiated by high-energy heavy ions with and without bias

Pei-Pei Hu[1,2,3] · Li-Jun Xu[1,3] · Sheng-Xia Zhang[1,3] · Peng-Fei Zhai[1,3] · Ling Lv[2] · Xiao-Yu Yan[1,3] · Zong-Zhen Li[1,3] · Yan-Rong Cao[2] · Xue-Feng Zheng[2] · Jian Zeng[1,2] · Yuan He[1,3] · Jie Liu[1,3]

Received: 27 November 2023 / Revised: 7 April 2024 / Accepted: 18 April 2024 / Published online: 20 December 2024

Abstract
Gallium nitride (GaN)-based devices have significant potential for space applications. However, the mechanisms of radiation damage to the device, particularly from strong ionizing radiation, remains unknown. This study investigates the effects of radiation on p-gate AlGaN/GaN high-electron-mobility transistors (HEMTs). Under a high voltage, the HEMT leakage current increased sharply and was accompanied by a rapid increase in power density that caused "thermal burnout" of the devices. In addition, a burnout signature appeared on the surface of the burned devices, proving that a single-event burnout effect occurred. Additionally, degradation, including an increase in the on-resistance and a decrease in the breakdown voltage, was observed in devices irradiated with high-energy heavy ions and without bias. The latent tracks induced by heavy ions penetrated the heterojunction interface and extended into the GaN layer. Moreover, a new type of N_2 bubble defect was discovered inside the tracks using Fresnel analysis. The accumulation of N_2 bubbles in the heterojunction and buffer layers is more likely to cause leakage and failure. This study indicates that electrical stress accelerates the failure rate and that improving heat dissipation is an effective reinforcement method for GaN-based devices.

Keywords GaN HEMTs · Heavy ions · Single-event burnout · Latent tracks · Degradation

1 Introduction

Gallium nitride (GaN)-based devices have great application potential because of their excellent functionality in high-frequency applications owing to their high mobility and saturation electron velocity. In particular, GaN-based power transistors are attractive candidates for space and aeronautics power applications owing to their wide bandgap and high critical electric field [1, 2]. GaN materials are considered highly resistant to radiation [3]; however, recent studies have shown that GaN-based devices are sensitive to displacement and ionization damage effects [4–7]. Of primary concern are the single-event burnout (SEB) effects in GaN-based devices during irradiation. Furthermore, differences between devices in the SEB response lead to a significant reduction in the rated voltages used in space equipment [8].

High-energy charged particles (high linear energy transfer (LET) particles with a high-energy loss) deposit energy on the path, resulting in a high density of ionization tracks, and electron–hole pairs are collected by the action of the electric field, forming a larger current signal. Charge generation and

This work was supported by the National Natural Science Foundation of China (Nos.12035019, 62234013, 12205350, 12075290, 12175287), the China National Postdoctoral Program for Innovative Talents (BX20200340), the fund of Innovation Center of Radiation Application (No. KFZC2022020601), and the Chinese Academy of Sciences (CAS) “Light of West China" Program hosted by Jian Zeng.

✉ Jian Zeng
zengjian@impcas.ac.cn

✉ Jie Liu
j.liu@impcas.ac.cn

1 Institute of Modern Physics, Chinese Academy of Sciences (CAS), Lanzhou 730000, China

2 Key Laboratory of Wide Band-gap Semiconductor Materials, Ministry of Education, Xidian University, Xi’an 710071, China

3 University of Chinese Academy of Sciences (UCAS), Beijing 100049, China

collection can cause soft or hard errors in the devices or integrated circuits [9–19], resulting in functional interruptions and performance failures. GaN-based high-electron-mobility transistors (HEMTs) exhibit enhanced leakage at high fluences. For example, in a single-event transient (SET) test, the leakage gradually increases as voltage increases. A higher LET also has a reinforcing effect. Considering the range and LET of the incident ions, only single-event effects (SEEs) induced by heavy ions and protons are usually considered. Heavy ions caused by device leakage are currently the main concern because the high fluence of heavy ions usually cannot occur in a space environment, and a high LET and voltage are the key factors affecting the SEE of the device [20, 21]. Heavy ions in the space environment can also cause an SEB effect in SiC-based metal-oxide semiconductor field-effect transistors (MOSFETs) [22, 23]. However, bipolar transistors are not included in GaN-based HEMTs and the SEB mechanism is different. A high LET and voltage results in lower device burn-out voltage thresholds and variation between devices, thereby resulting in greater voltage derating in space applications [24, 25]. Therefore, studying the failure mechanism of a device exposed to irradiation under controlled bias is essential for device reinforcement and space applications.

Recently, several studies have been conducted on the effects of radiation on GaN-based devices without bias. Their findings provide valuable original information on the defects induced in irradiated devices and prove that performance degradation is closely associated with material damage [26–28]. When high-energy heavy ions are incident on a solid material, their energy deposition induces a thermal spike along the ion trajectory, resulting in the formation of latent tracks with cylindrical or conical shapes and different morphologies [29–31]. In this process, different types of defects, such as vacancies and stress, are introduced, which have different effects on the irradiated devices. For example, changes in the lattice and piezoelectric constants can alter the Schottky contact, and high-density dislocations can increase the leakage current in the device [32, 33]. Additionally, the accumulation of principal defects such as N vacancies at the dislocation edge leads to enhanced conductivity in the ion collision region, increasing the chance of leakage and failure [34]. In this paper, we report on the radiation effects in AlGaN/GaN HEMTs induced by high-energy heavy ions, exploring the failure mechanism of devices with and without bias and establishing a deeper understanding of the effects of tracks on device failure to accurately predict device performance before testing.

2 Experiments section

In this study, AlGaN/GaN E-mode HEMTs manufactured by Xiamen Junmek Electronic Technology Co., Ltdẇere selected as the devices under test (DUTs). The device model used was SMG060E010L. The parameters of the device including breakdown voltage (BV_{DS}), on-resistance (R_{ON}), saturated output current ($I_{D,max}$), threshold voltage (V_{th}), and leakage current ($I_{D,leakage}$) are presented in Table 1. The DUTs included both bare chips and packaged devices. Before the irradiation experiments, the packages of the devices were removed via acid etching to ensure that the incident ions reached the sensitive areas of the DUTs. Subsequently, the electrical properties of each unsealed device were measured to select qualified samples. Figure 1a shows a photograph of a DUT after the package was removed. The cross-sectional diagram and structure characterized with scanning electron microscopy (SEM) are shown in Fig. 1b, c, respectively.

Heavy ion irradiation experiments were conducted at the Heavy Ion Research Facility in Lanzhou (HIRFL). The unsealed devices were irradiated with Ta ions in the off-state. The range of 2006 MeV Ta ions in GaN is 57.9 µm, which allows penetration through the heterojunctions and epitaxial layers. The specific irradiation parameters calculated using the SRIM-2013 code [35] are listed in Table 2. All the experiments were performed at room temperature. The flux was set as 1×10^4 ions/cm$^2 \cdot$ s for normal incidence. The test system consisted of two high-power system source meter instruments and software. Gate and drain biases were applied using Keithley 2651 and 2657 source meters, respectively. Source meters were also used to periodically monitor the gate leakage current (I_{gs}) and drain leakage current (I_{ds}) during the measurement, with a sampling time of approximately 0.05 s. During irradiation, the DUTs were biased to the off state with a high drain-source voltage V_{ds}. To obtain the burn-out voltage of the DUTs, V_{ds} was gradually

Table 1 Specifications of AlGaN/GaN HEMTs tested in this study

Item (T = 25 °C)	Specified value
BV_{DS} (V)	650
$I_{D,max}$ (A)	15
R_{ON} (mΩ)	100–150
V_{th} (V)	0.8–1.2
$I_{D,leakage}$ (µA)	5–20

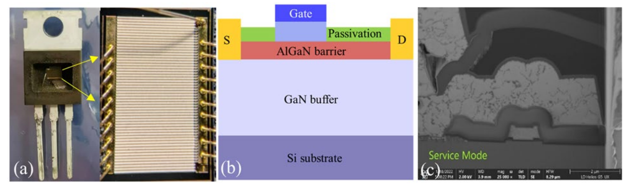

Fig. 1 (Color online) **a** Picture of a device under test after removing the package shell, **b** cross-sectional diagram, and **c** the structure of the device under test characterized with SEM imaging

Table 2 Experiment irradiation parameters, LET denotes the linear energy transfer in GaN and Si

Ions	Energy (MeV)	LET [MeV/(mg/cm^2)]		$(\mathrm{d}E/\mathrm{d}x)_e$ (keV/nm)	Range (μm)	Bias condition
		GaN	Si	GaN	GaN	
^{181}Ta	2006	59.9	75.4	36.8	57.9	With bias
^{129}Xe	450	52.9	69.2	32.6	20.0	Ground
^{209}Bi	780	76.2	99.5	46.9	24.7	Ground

$(\mathrm{d}E/\mathrm{d}x)_e$ denotes the electronic energy loss in GaN, as calculated with SRIM-2013 code [35]

increased from 0 V to 650 V, and the voltage growth step was adjusted according to the increase in leakage current. The software used in the test allowed setting current limitations to protect the source meters from burning out. The current measurement accuracy of the test system was on the order of 1 nA. I_{ds} and I_{gs} are displayed simultaneously to monitor the leakage current components. The DUTs were considered burned out with a leakage current greater than 20 mA during irradiation. Six groups of DUTs were irradiated in the heavy-ion irradiation experiments.

Bare chips were irradiated with 780 MeV Bi and 450 MeV Xe ions. The irradiation experiments were performed under vacuum conditions, and all terminals of the devices were grounded during testing. The specific irradiation parameters for GaN are listed in Table 2. Five devices were irradiated under each test condition to avoid the influence of part-to-part variations. The electrical parameters of the devices before and after irradiation were measured using a power device analyzer/curve tracer (Keysight B1505A). Transmission electron microscopy (TEM) was used to study structural modifications in the devices. Cross-sectional slices of the devices selected for the TEM and SEM measurements were prepared using a focused ion beam system (FIB).

3 Results and discussion

3.1 Single event burnout

Figure 2 shows the experimental results for devices irradiated with 2006 MeV Ta ions. The variations in I_{ds} and I_{gs} during irradiation as functions of time with $V_{gs} = -0.3$ V are shown in Fig. 2a, b, respectively. The V_{ds} was set to increase incrementally. An increase of two orders of magnitude in the leakage current I_{ds} was detected at $V_{ds} \geq 150$ V. In this process, the leakage current I_{gs} changed almost synchronously with I_{ds} and finally, the device was destroyed at 380 V with a sharp increase in the drain current $I_{ds} > 20$ mA). Apparent burnout signatures were observed on the chip surface, indicating that the device underwent an SEB.

To observe these failure modes, the maximum fluence level for each irradiation was fixed at 1×10^7 ions/cm^2, with maximum V_{ds} levels ranging from 350 V to 390 V. The gate voltage was set to either −0.3 V or –3 V. The leakage currents of the different devices increased relatively consistently, and catastrophic failures were observed in all cases. The variations in burnout voltage and gate bias are shown in Fig. 2c. The statistical experimental results indicate that the burnout voltage was approximately 60% of the rated voltage. Furthermore, the greater the gate bias, the lower the burnout voltage. The variations in burnout voltage and ion fluences are shown in Fig. 2d. The cumulative irradiation fluence of the burned device was distributed between 1×10^6 ions/cm^2 and 1×10^7 ions/cm^2. The V_{ds} dependence of the fluence that causes the SEB was not observed owing to individual differences in the device.

To further investigate the failure mechanism of the burned devices, microregion localization and cross-sectional analysis of the devices irradiated by Ta ions were performed using FIB sampling and SEM. The burned areas are represented by black lines and molten pits in Fig. 3a, as observed using optical microscopy and photoemission microscopy (PEM). Figure 3b shows a cross-sectional view of the damaged location observed using SEM. High-resolution images of the yellow and white dashed boxes in Fig. 3b are shown in Fig. 3c, d, respectively. In addition to the thermal damage generated in the drain electrode, a portion of the region bridging the drain and source was blown into the body. The molten matter penetrated the heterojunction region into the GaN buffer layer, and the near-surface material of the device melted after burning. The heterojunction channels and the GaN buffer layer under the electrode were severely damaged. This shows that the high voltage aggravates the burn rate of the device. Under a high voltage, the leakage current increased sharply, accompanied by a rapid increase in power density, which in turn caused "thermal burnout". This type of catastrophic damage has two distinct characteristics: (1) A burnout signature was identified on the surface of the chip, and (2) a sudden increase in I_{gs} occurred when the devices burned out, because there was a short circuit between the gate and drain [36]. Furthermore, no latent tracks were observed, as shown in Fig. 3d, because the maximum cumulative irradiation fluences of the burned device were lower than 1×10^7 ions/cm^2 (0.1 ions/μm^2).

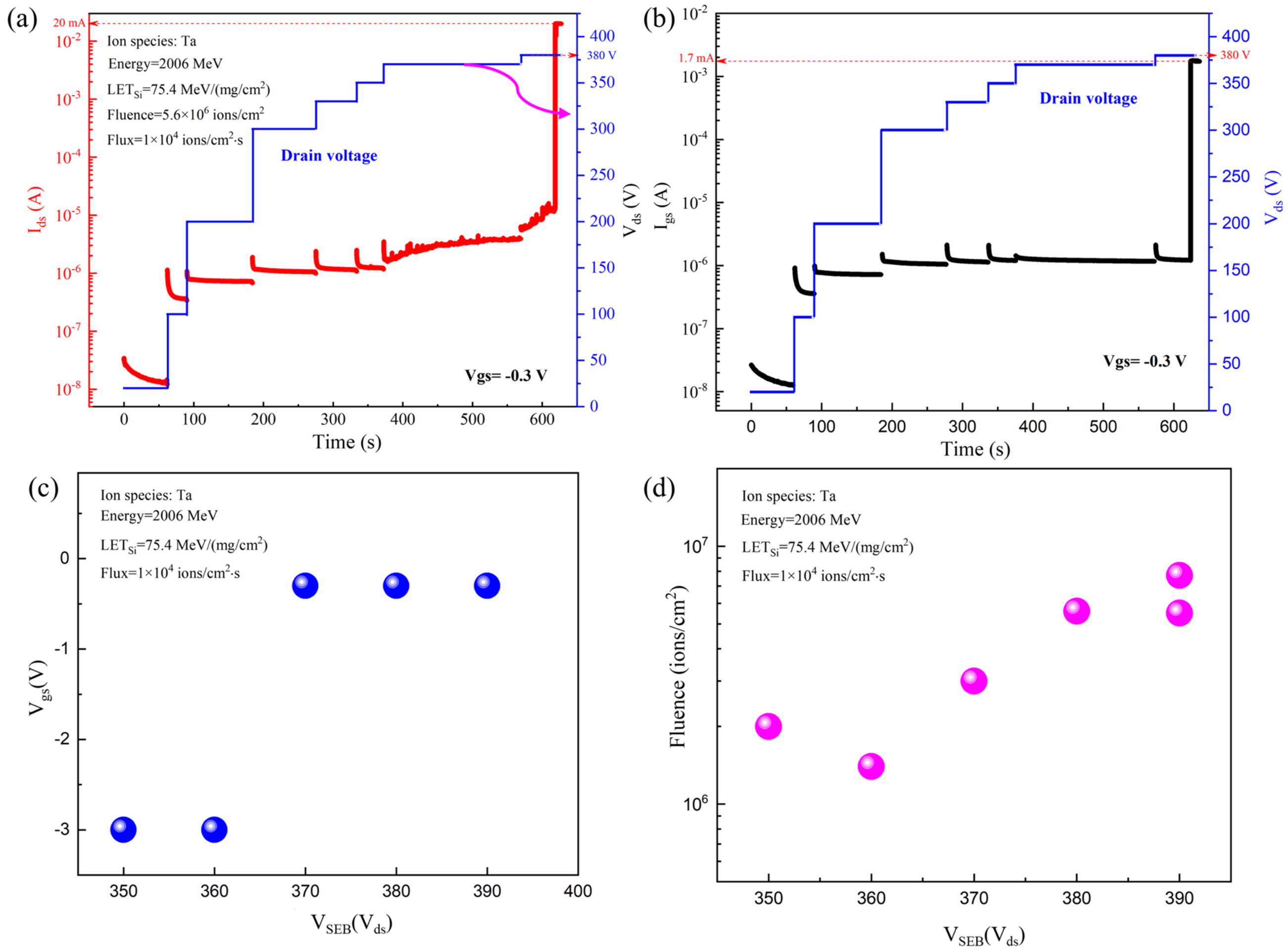

Fig. 2 Variation of the leakage current **a** I_{ds} and **b** I_{gs} as a function of time during the irradiation of Ta ions. Variation between **c** the single-event burnout voltage (V_{SEB}) with gate bias and **d** with ion fluences in the devices irradiated by Ta ions

3.2 Degradation of performance

The chips were irradiated with 780 MeV Bi and 450 MeV Xe ions without bias (all terminals were grounded). The transfer characteristics (I_{ds} vs. V_{gs}) of the devices are shown in Fig. 4a, b. In the case of Bi-ion irradiation, the threshold voltage V_{gs} shifted positively with an increase in the ion fluence, and the slope of the curve decreased. This implies that the switching characteristics were degenerate. However, no significant degradation was observed for the devices irradiated with 450 MeV Xe ions at fluences below 1×10^{10} ions/cm^2. Additionally, the drain current decreased to 0 when the ion fluence reached 1×10^{11} ions/cm^2, for both Bi- and Xe-ion irradiation. This suggests that the irradiated devices failed because of defects induced by high-energy heavy ions. Irradiation-induced defects are known to decrease the concentration of channel carriers and lead to a shift in threshold voltage [37–39]. From previous research, the sheet carrier density of a 2-D electron gas (2-DEG) n_s can be calculated by [40]

$$n_s = \frac{\epsilon}{qd}\left(V_{gs} - V_{th} - \frac{E_F}{q}\right), \tag{1}$$

where ϵ is the dielectric constant of the AlGaN layer, d is the distance between the gate and the sheet charge, V_{gs} is the gate-to-source voltage, V_{th} is the threshold voltage, and E_F is the Fermi energy in the two-dimensional potential well. The threshold voltage calculated from the transfer characteristics shifted toward positive values, as shown in Fig. 4c. This suggests that the 2-DEG is depleted and the properties of the devices deteriorated with heavy-ion irradiation. As the gate voltage exceeded the threshold value, the Fermi energy in the potential well increased, resulting in a decrease in n_s. Furthermore, a reduction in n_s significantly degraded the electrical performance of irradiated devices. Moreover, the

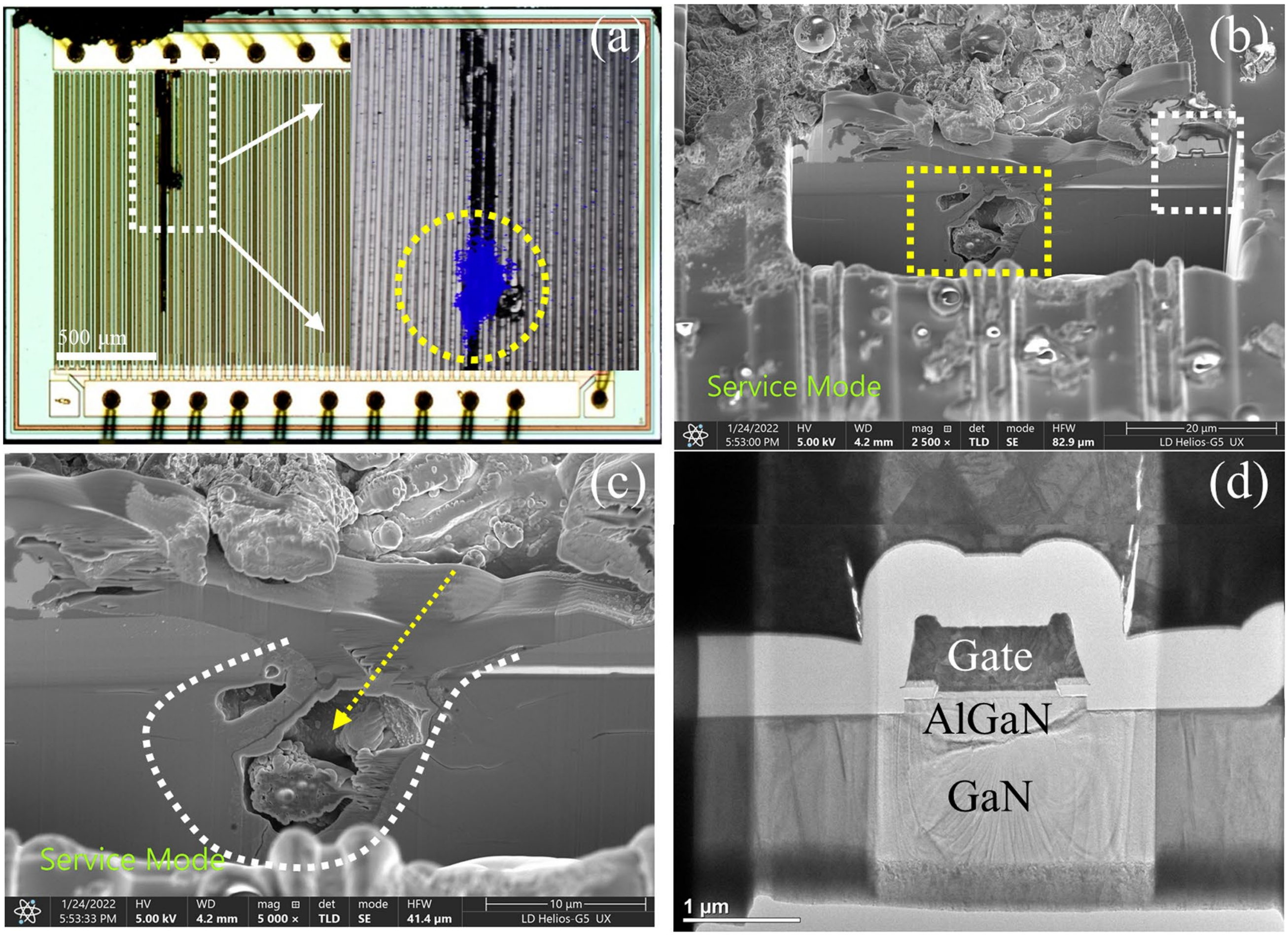

Fig. 3 (Color online) Damage site for burned devices. **a** Top view from optical microscopy and PEM, **b** cross-sectional view of the damage site examined by SEM, **c** magnification of areas marked by the yellow dashed box in **b**, and **d** TEM images of areas marked by the white dashed box in **b**

degradation caused by Bi ions was more severe than that of Xe ions, which is attributed to the $(\mathrm{d}E/\mathrm{d}x)_\mathrm{e}$ of the high-energy heavy ions.

The output characteristics of the devices irradiated with Bi and Xe are shown in Fig. 4d, e, respectively, measured at $V_{gs} = 4$ V. The saturation current degraded significantly and the threshold voltage V_{ds} for the curves entering the saturation region was reduced with increasing ion fluence in the case of Bi-ion irradiation. The variation in the saturation current in the devices irradiated with Xe was similar to that caused by Bi ions; however, the reduction rate was much lower. Although the drain current I_{ds} decreased with different amplitudes, it decreased to zero when the ion fluence reached 1×10^{11} ions/cm^2, with both Bi- and Xe-ion irradiation. The on-resistance R_{on} calculated from the output characteristics increased significantly, as shown in Fig. 4f. The value of R_{on} increased with increasing ion fluence for both Xe and Bi ions and eventually increased to infinity when the ion fluence reached 1×10^{11} ions/cm^2. These results demonstrated that the devices failed. Figure 4g, h shows the characteristic breakdown curves for different fluences before and after irradiation. The BV_{DS} of the device before irradiation was greater than 650 V, and did not show significant degradation up to a fluence of 5×10^9 ions/cm^2 when irradiated with Xe ions. When the ion fluence was increased to 1×10^{10} ions/cm^2, BV_{DS} sharply reduced to 100 V. Moreover, BV_{DS} approached 0 as the ion fluence increased to 1×10^{11} ions/cm^2. For Bi-ion irradiation, BV_{DS} decreased rapidly. As the ion fluence increased to 5×10^8 ions/cm^2, BV_{DS} reduced to 110 V and reduced to 0 as the ion fluence increased to 1×10^{10} ions/cm^2, as shown in Fig. 4i. This is consistent with the changes in the transfer and output characteristics and confirms that the devices degraded at low fluences and failed at high fluences under the irradiation of high-energy heavy ions.

With an increase in the ion fluence, defects or clusters of defects induced by irradiation accumulate in the 2-DEG

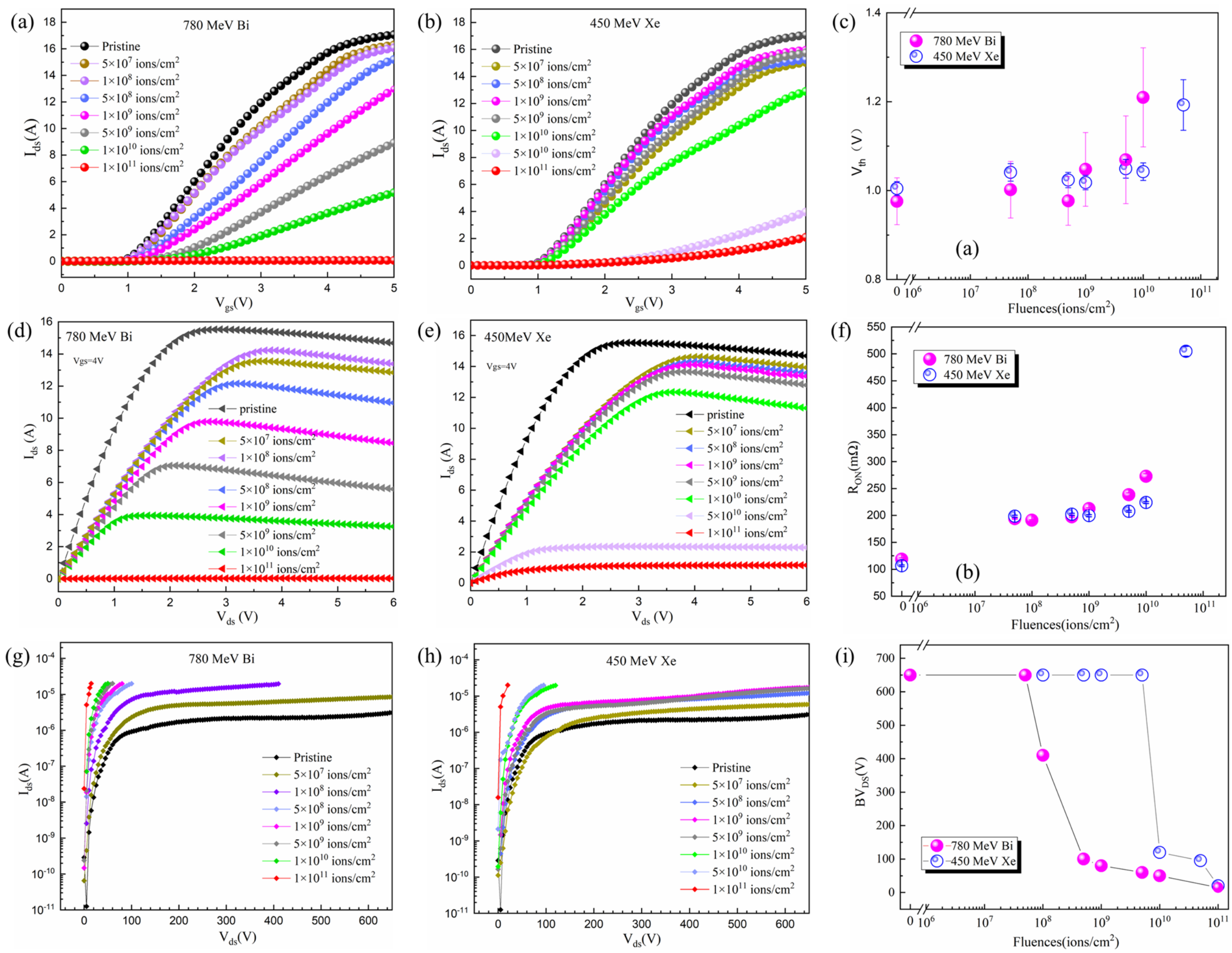

Fig. 4 (Color online) Electrical properties of AlGaN/GaN HEMTs before and after irradiation. Transfer characteristics for **a** 780 MeV Bi and **b** 450 MeV Xe ion irradiation. **c** Evolution of threshold voltage V_{th} with ion fluence. Output characteristics for **d** 780 MeV Bi and **e** 450 MeV Xe ion irradiation. **f** Evolution of on-resistance R_{ON} with ion fluence. Breakdown voltage for **g** 780 MeV Bi and **h** 450 MeV Xe ion irradiation. **i** Evolution of breakdown voltage BV_{DS} with ion fluence

channel, resulting in structural disorders, modification of the electrical parameters, and degradation of the electrical performance of the device. Additionally, the devices were measured after irradiation, and six months later, their performance did not recover. This implies that no annealing effect occurred at room temperature and confirms that the high-energy heavy-ion irradiation induced permanent damage inside the device. Moreover, the performance degradation was more significant in devices irradiated with Bi ions than in those irradiated with Xe ions. The electronic energy loss $(\mathrm{d}E/\mathrm{d}x)_e$ of Bi ions (46.9 keV/nm) in GaN is higher than that of Xe ions. This indicates that the greater the $(\mathrm{d}E/\mathrm{d}x)_e$, the more serious the performance degradation of the device. In addition, the higher the ion fluence, the more structural damage occurs, which eventually results in device failure. Therefore, $(\mathrm{d}E/\mathrm{d}x)_e$ and ion fluences are the key factors that cause device degradation without a bias effect [41, 42].

3.3 Irradiation-induced latent tracks

Damaged sites on the surfaces of chips irradiated without bias cannot be observed directly by optical microscopy. To further investigate the failure mechanism during irradiation, microregion localization and cross-sectional analysis of the DUTs irradiated by 780 MeV Bi with a fluence of 1×10^{11} ions/cm^2 were performed using FIB sampling and TEM. Figure 5a shows the T-shaped gate regions of the irradiated samples. The regions under the gate electrode, marked by red boxes, are shown in Fig. 5b, c. Dark line-shaped latent tracks extending from the AlGaN/GaN heterojunction channel to the GaN buffer layer were introduced. Latent tracks were also observed between the drain and gate electron regions. Figure 5d shows an oriented TEM image of the device. The regions marked by the red box were observed at high magnification and different focus depths,

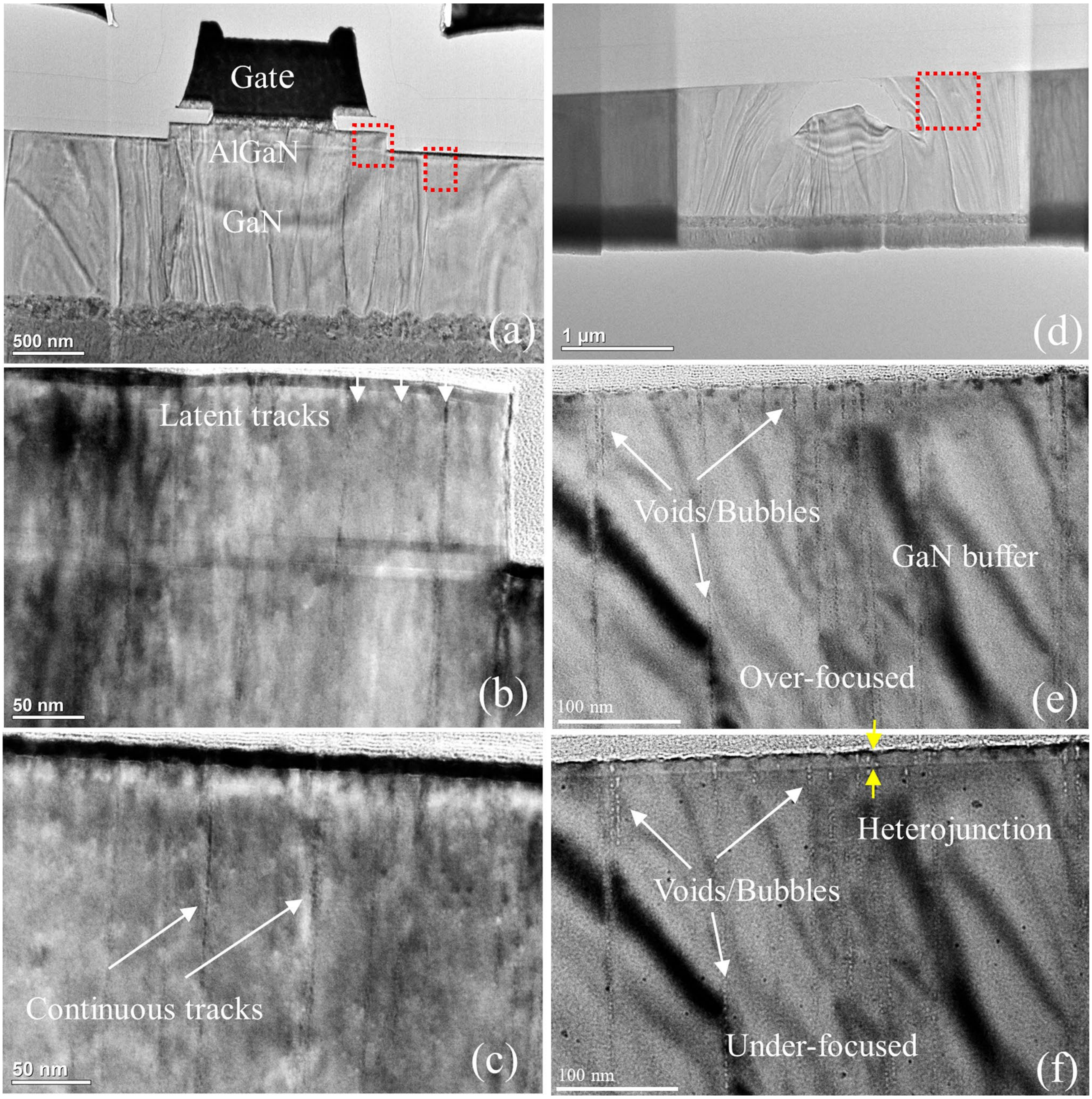

Fig. 5 Cross-sectional images in AlGaN/GaN high-electron-mobility transistors caused by 780 MeV Bi ions at a fluence of 1×10^{11} ions/cm^2. **a**–**c** Latent tracks under gate regions with different resolutions. **d**–**f** Fresnel analysis around the latent tracks induced in the AlGaN/GaN heterojunction and GaN buffer layers

as shown in Fig. 5e, f. The tracks generated at different locations penetrated the GaN buffer layer of the device. According to previous experimental results, the $(dE/dx)_e$ threshold for latent track formation in bulk GaN crystal is approximately 15–22 keV/nm [43, 44]. For the 780 MeV Bi ions used in this study, $(dE/dx)_e$ was approximately 46.9 keV/nm when the incident ions reached the heterojunction interface, producing distinguishable and continuous tracks in the irradiated devices. The most notable difference is the formation of N_2 bubbles inside the tracks created by 780 MeV Bi ions that do not appear with lower-energy ions, as shown in Fig. 5f. The N_2 bubbles induced in the heterojunction and buffer layer were clearly identified, as predicted by a two-temperature model-molecular dynamics (TTM-MD) simulation [45, 46]. This uniform distribution with different depths confirms that the N_2 bubbles formed instead of voids because the formation of voids requires a large amount of material to flow upward, followed by sputtering.

For heavy ions with low-to-medium energies, although the temperature was extremely high, the coexisting pressure within the tracks maintained most of the GaN material in a consistent melting state, except for the formation of a small number of N_2 molecules to form split interstitials. In contrast, the temperature and pressure generated by high-energy heavy ions results in a portion of the heated material being separated and decomposed into N_2 and Ga molecules. These molecules combine to form bubbles during cooling [47, 48]. This process is irreversible because the strong binding of the N_2 bubbles maintains a stable state after reaching room temperature. Similar structures were observed in the TEM images of 4.5 MeV/amu Pb with $(\mathrm{d}E/\mathrm{d}x)_\mathrm{e}$ values of 46 keV/nm [49]. With the penetration of high-energy heavy ions, an amorphous core forms along the tracks, and the pressure induced in the surrounding structure can be attributed to the Poisson effect, which results in longitudinal expansion under transverse compressive stress [50, 51]. Lattice expansion can influence the bandgap, piezoelectric properties, and resistance of materials [32, 33]. Therefore, latent tracks induced by heavy ions are critical factors in device degradation.

As scattering centers, the latent tracks increase with irradiation fluence, eventually leading to a significant decrease in the concentration of the active carriers, weakening of the gate-voltage controllability, and a shift in the threshold voltage [52]. Radiation defects in the channel also influence the electrical performance. These defects in the channel can decrease the height of the heterojunction barrier, resulting in a decrease in n_s in the 2-DEG and an increase in the resistivity, eventually leading to a positive shift in the threshold and degradation in the saturation leakage current. Furthermore, the accumulation of N_2 bubbles could speculatively lead to the formation of high-density nitrogen vacancies along the tracks, leading to enhanced conductivity of the track regions [53, 54], which is more likely to induce a leakage channel and result in the catastrophic failure of devices irradiated by high-energy heavy ions.

During the formation of the tracks, when the temperature of the crystal exceeds its melting point, a solid–liquid phase transformation (phase I) is formed, which cools down with the partially recovered crystal by recrystallization (phase II) [55]. As reported by Sequeira et al. [46], 185 MeV Au ions can create a cylindrical molten track in phase I and induce an amorphous core in phase II in GaN crystals. The radius of the molten track is 4.4 nm with a core radius of 1.8 nm. Clearly, over 80% of the crystal volume initially influenced by the incidence of a single high-energy heavy ion is eventually recovered by recrystallization. Therefore, the crystal structures were strongly modified by high-energy heavy ions, even at low fluences. Furthermore, devices irradiated with Ta ions with bias failed at much lower fluences (1×10^6–1×10^7 ions/cm^2) than those without bias. At the same ion fluences, there is no obvious degradation for Bi-ion irradiation without bias, although the Bi ions have a much higher $(\mathrm{d}E/\mathrm{d}x)_\mathrm{e}$. It can be concluded that electrical stress accelerates the failure rate during irradiation.

4 Conclusion

In this study, the failure mechanisms of AlGaN/GaN HEMTs with and without bias were investigated. In the SEB experiments, the incident ions produced high-density carriers through the ionization or excitation effect, and a large current pulse was formed under a high voltage between the drain and source. The device power density increased sharply and the local temperature rose. Beyond the melting point of the crystal, a "hot" burnout occurs and results in a permanent damage. For devices irradiated without bias, the performance degradation was closely related to the fluence and $(\mathrm{d}E/\mathrm{d}x)_\mathrm{e}$. The new N_2 bubble defects accumulated at the heterojunction and the buffer layers are likely to induce a leakage channel, resulting in the failure of devices irradiated without bias. The results indicate that electrical stress accelerates the failure rate and provide direct evidence that heat dissipation is an effective reinforcement method for GaN-based devices.

Author contributions All authors contributed to the study conception and design. Material preparation, data collection and analysis were performed by Pei-Pei Hu, Li-Jun Xu, Peng-Fei Zhai, Ling Lv, and Xiao-Yu Yan. The first draft of the manuscript was written by Pei-Pei Hu and all authors commented on previous versions of the manuscript. All authors read and approved the final manuscript.

Data availability The data that support the findings of this study are openly available in Science Data Bank at https://cstr.cn/31253.11.sciencedb.j00186.00281 and https://doi.org/10.57760/sciencedb.j00186.00281.

Declarations

Conflict of interest Yuan He is an editorial board member for Nuclear Science and Techniques and was not involved in the editorial review, or the decision to publish this article. All authors declare that there are no conflict of interest.

References

1. T.P. Chow, R. Tyagi, Wide bandgap compound semiconductors for superior high-voltage unipolar power devices. IEEE Trans. Electron Dev. Sci. **41**, 1481–1483 (1994). https://doi.org/10.1109/ISPSD.1993.297113
2. W. Saito, Y. Takada, M. Kuraguchi et al., High breakdown voltage AlGaN/GaN power-HEMT design and high current density switching behavior. IEEE Trans. Electron Dev. Sci. **50**, 2528–2531 (2003). https://doi.org/10.1109/TED.2003.819248

3. S.J. Pearton, F. Ren, E. Patrick et al., Review-Ionizing radiation damage effects on GaN devices. ECS J. Solid State Sci. Technol **5**, Q35–Q60 (2016). https://doi.org/10.1149/2.0251602jss
4. Z.G. Wang, Y.F. Jin, Effective energy deposition and latent track formation of swift heavy ions in solids. Nucl. Sci. Tech. **16**, 12–16 (2005)
5. A.Y. Polyakov, S.J. Pearton, P. Frenzer et al., Radiation effects in GaN materials and devices. J. Mater. Chem. C. Sci. **5**, 877–887 (2013). https://doi.org/10.1039/C2TC00039C
6. L.Q. Zhang, C.H. Zhang, C.L. Xu et al., Damage produced on GaN surface by highly charged Kr^{q+} irradiation. Nucl. Sci. Tech. **28**, 176 (2017). https://doi.org/10.1007/s41365-017-0326-4
7. G.P. Liu, X. Wang, M.N. Li et al., Effects of high-energy proton irradiation on separate absorption and multiplication GaN avalanche photodiode. Nucl. Sci. Tech. **29**, 139 (2018). https://doi.org/10.1007/s41365-018-0480-3
8. M.J. Martinez, M.P. King, A.G. Baca et al., Radiation response of AlGaN-channel HEMTs. IEEE Trans. Nucl. Sci. **66**, 344–351 (2019). https://doi.org/10.1109/TNS.2018.2885526
9. Z. He, S.W. Zhao, T.Q. Liu et al., Verification of SEU resistance in 65 nm high-performance SRAM with dual DICE interleaving and EDAC mitigation strategies. Nucl. Sci. Tech. **32**, 139 (2021). https://doi.org/10.1007/s41365-021-00979-8
10. S. Gao, J.H. Yang, B. Ye et al., Differences in MBUs induced by high-energy and medium-energy heavy ions in 28 nm FPGAs. Nucl. Sci. Tech. **33**, 112 (2022). https://doi.org/10.1007/s41365-022-01099-7
11. D.M. Fleetwood, Radiation Effects in AlGaN/GaN HEMTs. IEEE Trans. Nucl. Sci. **69**, 1105–1119 (2022). https://doi.org/10.1109/TNS.2022.3147143
12. T. Tong, X.H. Wang, Z.G. Zhang et al., Effectiveness and failure modes of error correcting code in industrial 65 nm CMOS SRAMs exposed to heavy ions. Nucl. Sci. Tech. **25**, 010405 (2014). https://doi.org/10.13538/j.1001-8042/nst.25.010405
13. C. Cai, T.Q. Liu, X.Y. Li et al., Heavy-ion and pulsed-laser single event effects in 130-nm CMOS-based thin/thick gate oxide anti-fuse PROMs. Nucl. Sci. Tech. **30**, 80 (2019). https://doi.org/10.1007/s41365-019-0602-6
14. X.B. Cao, L.Y. Xiao, M.X. Huo et al., Heavy ion-induced single event upset sensitivity evaluation of 3D integrated static random access memory. Nucl. Sci. Tech. **29**, 31 (2018). https://doi.org/10.1007/s41365-018-0377-1
15. Z.L. Yang, X.H. Wang, H. Su et al., Experimental study on heavy ion single-event effects in flash-based FPGAs. Nucl. Sci. Tech. **27**, 7 (2016). https://doi.org/10.1007/s41365-016-0015-8
16. L. Cai, G. Guo, J.C. Liu et al., Experimental study of temperature dependence of single-event upset in SRAMs. Nucl. Sci. Tech. **27**, 16 (2016). https://doi.org/10.1007/s41365-016-0014-9
17. W.T. Yang, X.C. Du, Y.H. Li et al., Single-event-effect propagation investigation on nanoscale system on chip by applying heavy-ion microbeam and event tree analysis. Nucl. Sci. Tech. **32**, 106 (2021). https://doi.org/10.1007/s41365-021-00943-6
18. J.Y. Xu, S.M. Chen, R.Q. Song et al., Analysis of single-event transient sensitivity in fully depleted silicon-on-insulator MOSFETs. Nucl. Sci. Tech. **29**, 49 (2018). https://doi.org/10.1007/s41365-018-0391-3
19. J. Liu, Z. Zhou, D. Wang et al., Prototype of single-event effect localization system with CMOS pixel sensor. Nucl. Sci. Tech. **33**, 136 (2022). https://doi.org/10.1007/s41365-022-01128-5
20. S. Gao, X.Y. Li, S.W. Zhao et al., Heavy ion-induced MCUs in 28 nm SRAM-based FPGAs: upset proportions, classifications, and pattern shapes. Nucl. Sci. Tech. **33**, 161 (2022). https://doi.org/10.1007/s41365-022-01142-7
21. S. Liu, M. Boden, D.A. Girdhar et al., Single-event burnout and avalanche characteristics of power DMOSFETs. IEEE Trans. Nucl. Sci. **53**, 3379–3385 (2006). https://doi.org/10.1109/TNS.2006.884971
22. A. Akturk, R. Wilkins, J. McGarrity et al., Single event effects in Si and SiC power MOSFETs due to terrestrial neutrons. IEEE Trans. Nucl. Sci. **64**, 529–535 (2017). https://doi.org/10.1109/TNS.2016.2640945
23. A.F. Witulski, D.R. Ball, K.F. Galloway et al., Single-event burnout mechanisms in SiC power MOSFETs. IEEE Trans. Nucl. Sci. **65**, 1951–1955 (2018). https://doi.org/10.1109/TNS.2018.2849405
24. S. Kuboyama, C. Kamezawa, N. Ikeda et al., Anomalous charge collection in silicon carbide Schottky barrier diodes and resulting permanent damage and single-event burnout. IEEE Trans. Nucl. Sci. **53**, 3343–3348 (2006). https://doi.org/10.1109/TNS.2006.885165
25. D.R. Ball, J.M. Hutson, A. Javanainen et al., Ion-induced energy pulse mechanism for single-event burnout in high-voltage SiC power MOSFETs and junction barrier Schottky diodes. IEEE Trans. Nucl. Sci. **67**, 22–28 (2020). https://doi.org/10.1109/TNS.2019.2955922
26. P.P. Hu, J. Liu, S.X. Zhang et al., Degradation in AlGaN/GaN HEMTs irradiated with swift heavy ions: role of latent tracks. Nucl. Instrum. Meth. B **430**, 59–63 (2018). https://doi.org/10.1016/j.nimb.2018.06.011
27. P. Hazdra, S. Popelka, Radiation resistance of wide-bandga P semiconductor power transistors. Phys. Status Solidi A **214**, 1600447 (2016). https://doi.org/10.1002/pssa.201600447
28. P.F. Wan, J.Q. Yang, T. Ying et al., Effects of ionization and displacement damage in AlGaN/GaN HEMT devices caused by various heavy ions. IEEE Trans. Nucl. Sci. **68**, 1265–1271 (2021). https://doi.org/10.1109/TNS.2021.3074391
29. A. Kamarou, W. Wesch, E. Wendler et al., Swift heavy ion irradiation of InP: thermal spike modeling of track formation. Phys. Rev. Condens. B Matter Mater. Phys. **73**, 184107 (2006). https://doi.org/10.1103/PhysRevB.73.184107
30. W.J. Weber, D.M. Duffy, L. Thome et al., The role of electronic energy loss in ion beam modification of materials. Solid State Mater. Sci. **19**, 1–11 (2015). https://doi.org/10.1016/j.cossms.2014.09.003
31. P.F. Zhai, S. Nan, L.J. Xu et al., Fine structure of swift heavy ion track in rutile TiO_2. Nucl. Instrum. Methods B **457**, 72–79 (2019). https://doi.org/10.1016/j.nimb.2019.07.024
32. J.W.P. Hsu, M.J. Manfra, R.J. Molnar et al., Direct imaging of reverse-bias leakage through pure screw dislocations in GaN films grown by molecular beam epitaxy on GaN templates. Appl. Phys. Lett. **81**, 79–81 (2002). https://doi.org/10.1063/1.1490147
33. S.W. Kaun, M.H. Wong, S. Dasgupta et al., Effects of threading dislocation density on the gate leakage of AlGaN/GaN heterostructures for high electron mobility transistors. Appl. Phys. Express **4**, 024101 (2011). https://doi.org/10.1143/APEX.4.024101
34. J. Elsner, R. Jones, M.I. Heggie et al., Deep acceptors trapped at threading-edge dislocations in GaN. Phys. Rev. B Condens. Matter **58**, 12571–12574 (2002). https://doi.org/10.1103/PhysRevB.58.12571
35. J.F. Ziegler, M.D. Ziegler, J.P. Biersack, SRIM—the stopping and range of ions in matter. Nucl. Instr. Methods B **268**, 1818–1823 (2010). https://doi.org/10.1016/j.nimb.2010.02.091
36. E. Mizuta, S. Kuboyama, Y. Nakada et al., Single-event damage observed in GaN-on-Si HEMTs for power control applications. IEEE Trans. Nucl. Sci. **65**, 1956–1963 (2018). https://doi.org/10.1109/TNS.2018.2819990
37. A. Kalavagunta, A. Touboul, L. Shen et al., Electrostatic mechanisms responsible for device degradation in proton irradiated AlGaN/AlN/GaN HEMTs. IEEE Trans. Nucl. Sci. **55**, 2106–2112 (2008). https://doi.org/10.1109/TNS.2008.2001705

38. T. Roy, E.X. Zhang, Y.S. Puzyrev et al., Process dependence of proton-induced degradation in GaN HEMTs. IEEE Trans. Nucl. Sci. **57**, 3060–3065 (2010). https://doi.org/10.1109/TNS.2010.2073720
39. S.T. Pantelides, Y. Puzyrev, X. Shen et al., Reliability of III–V devices—the defects that cause the trouble. Microelectron. Eng. **90**, 3–8 (2012). https://doi.org/10.1016/j.mee.2011.04.019
40. A.P. Karmarkar, B. Jun, D.M. Fleetwood et al., Proton irradiation effects on GaN-based high electron-mobility transistors with Si-doped AlxGaxN and Thick GaN cap layers. IEEE Trans. Nucl. Sci. **51**, 3801–3806 (2004). https://doi.org/10.1109/TNS.2004.839199
41. A. Kumar, R. Singh, P. Kumar et al., In-situ transport and microstructural evolution in GaN Schottky diodes and epilayers exposed to swift heavy ion irradiation. J. Appl. Phys. **123**, 161539 (2018). https://doi.org/10.1063/1.4995491
42. P.F. Wan, J.Q. Yang, G. Lv et al., Effect of hydrogen on radiation-induced displacement damage in AlGaN/GaN HEMTs. IEEE Trans. Nucl. Sci. **68**, 1258–1264 (2021). https://doi.org/10.1109/TNS.2021.3074379
43. M.A. Rana, A compound spike model for formation of nuclear tracks in solids. Nucl. Sci. Tech. **18**, 349–353 (2007). https://doi.org/10.1016/S1001-8042(08)60006-8
44. G. Schiwietz, P. Grande, Stopping of protons improved accuracy of the UCA model. Nucl. Instrum. Methods B **273**, 1–5 (2012). https://doi.org/10.1016/j.nimb.2011.07.023
45. N. Ishikawa, N. Okubo, T. Taguchi et al., Experimental evidence of crystalline hillocks created by irradiation of CeO2 with swift heavy ions. Nanotechnology **26**, 35570 (2015). https://doi.org/10.1088/0957-4484/26/35/355701
46. M.C. Sequeira, F. Djurabekova, K. Nordlund et al., Examining different regimes of ionization-induced damage in GaN through atomistic simulations. Small **18**, 2102235 (2022). https://doi.org/10.1002/smll.202102235
47. M.C. Sequeira, J.G. Mattei, H. Vazquez et al., Unravelling the secrets of the resistance of GaN to strongly ionising radiation. Commun. Phys. **4**, 1–8 (2021). https://doi.org/10.1038/s42005-021-00550-2
48. J.G. Mattei, M. Sall, F. Moisy et al., Fullerene irradiation leading to track formation enclosing nitrogen bubbles in GaN material. Materialia **15**, 100987 (2021). https://doi.org/10.1016/j.mtla.2020.100987
49. M. Sall, I. Monnet, F. Moisy et al., Track formation in III–N semiconductors irradiated by swift heavy ions and fullerene and reevaluation of the inelastic thermal spike model. J. Mater. Sci. **50**, 5214–5227 (2015). https://doi.org/10.1007/s10853-015-9069-y
50. P. Jozwik, J.P.S. Cardoso, D.F. Carvalho et al., Damage in InGaN/GaN bilayers upon Xe and Pb swift heavy ion irradiation. Phys. Chem. Chem. Phys. **42**, 25773–25787 (2022). https://doi.org/10.1039/D2CP02526D
51. P.P. Hu, J. Liu, S.X. Zhang et al., Raman investigation of lattice defects and stress induced in InP and GaN films by swift heavy ion irradiation. Nucl. Instrum. Methods B **372**, 29–37 (2016). https://doi.org/10.1016/j.nimb.2016.01.031
52. T.J. Anderson, A.D. Koehler, J.D. Greenlee et al., Substrate-dependent effects on the response of AlGaN/GaN HEMTs to 2-MeV proton irradiation. IEEE Electr. Dev. L **35**, 826–828 (2014). https://doi.org/10.1109/LED.2014.2331001
53. T. Hashizume, J. Kotani, H. Hasegawa et al., Leakage mechanism in GaN and AlGaN Schottky interfaces. Appl. Phys. Lett. **84**, 4884–4886 (2004). https://doi.org/10.1063/1.1762980
54. L.L. Chen, N. Jing, D.W. Yan et al., Charge transport in vertical GaN Schottky barrier diodes: a refined physical model for conductive dislocations. IEEE Trans. Electron Dev. **67**, 841–846 (2020). https://doi.org/10.1109/TED.2020.2965953
55. M. Toulemonde, C. Dufour, A. Meftah et al., Transient thermal processes in heavy ion irradiation of crystalline inorganic insulators. Nucl. Instrum. Methods B **166**, 903–912 (2000). https://doi.org/10.1016/S0168-583X(99)00799-5